Acta Pharmaceutica Sinica B 2026;16(7):4478−4490

Chinese Pharmaceutical Association
Institute of Materia Medica, Chinese Academy of Medical Sciences

Acta Pharmaceutica Sinica B

www.elsevier.com/locate/apsb
www.sciencedirect.com

ORIGINAL ARTICLE

A novel NAMPT activator ameliorates obesity by repressing ACSL1-dependent lipid synthesis

Zhi Jiang, Yi-Xian Li, Dan-Dan Zhao, Yu-Tao Hu, Ling-Zhen Xiao, Yu-Wei Lin, Shu-Min Xu, Jia-Chun Luo, Qingjiang Li, Shi-Liang Huang, Hui-Hao Zhou, Jia-Heng Tan, Shuo-Bin Chen*, Zhi-Shu Huang*

School of Pharmaceutical Sciences, Guangdong Provincial Key Laboratory of New Drug Design and Evaluation, Sun Yat-sen University, Guangzhou 510006, China

Received 3 September 2025; received in revised form 20 December 2025; accepted 5 February 2026

KEY WORDS

Obesity;
Metabolic disorder;
NAMPT;
NAD^+;
SIRT1;
ACSL1;
Long-chain fatty acids;
Triglyceride biosynthesis

Abstract Excessive incorporation of long-chain fatty acids (LCFAs) into triglycerides in adipose tissue is a key contributor to obesity and related metabolic disorders, and pharmacologically modulating this process remains challenging. Here, we synthesized a library of β-indoquinazolinone derivatives *via* palladium-catalyzed oxidative addition complex chemistry and identified compound b2b as a potent and selective anti-obesity candidate. b2b inhibited triglyceride accumulation in adipocytes *in vitro* and significantly reduced adiposity, body weight, and lipid metabolic disturbances in diet-induced obese mice without observable toxicity. Mechanistic studies revealed that b2b directly activates nicotinamide phosphoribosyltransferase (NAMPT) and elevates intracellular NAD^+ levels to enhance the NAD^+-dependent regulatory protein SIRT1 activity. This activation leads to transcriptional repression of acyl-CoA synthetase long-chain family member 1 (ACSL1), thereby inhibiting LCFAs incorporation into triglycerides. These findings demonstrate that pharmacological activation of the NAMPT-NAD^+-SIRT1 axis by b2b offers a novel strategy for obesity treatment.

*Corresponding authors.
E-mail addresses: chenshb8@mail.sysu.edu.cn (Shuo-Bin Chen), ceshzs@mail.sysu.edu.cn (Zhi-Shu Huang).

Peer review under the responsibility of Chinese Pharmaceutical Association and Institute of Materia Medica, Chinese Academy of Medical Sciences.

https://doi.org/10.1016/j.apsb.2026.03.039

1. Introduction

Adipose tissue plays a central role in systemic lipid homeostasis. In obesity, adipose depots exhibit dysregulated lipid metabolism, resulting in a chronic energy imbalance driven by excessive caloric intake relative to expenditure[1]. This sustained positive energy balance activates anabolic lipid pathways, leading to pathological triglycerides (TGs) accumulation in adipocytes. Current anti-obesity therapies, such as glucagon-like peptide-1 (GLP-1) receptor agonists, primarily function by suppressing appetite to reduce energy intake[2]. However, obesity is a multifactorial metabolic disorder involving excess TGs storage that results from dysregulated lipid handling across various tissues[3]. Therefore, the identification of adipose-specific molecular targets and development of molecules capable of modulating lipid storage represent critical avenues for precision metabolic reprogramming in obesity treatment.

TG biosynthesis is fundamental for energy storage in adipocytes[4]. In obesity, this process becomes pathologically enhanced due to increased de novo lipogenesis (DNL), TG biosynthesis, and lipid droplet formation[5]. The heightened fatty acid (FA) production machinery drives preferential esterification into TGs, promoting adipocyte lipids accumulation. These changes promote adipocyte hypertrophy and hyperplasia, contributing to local inflammation, hypoxia, and systemic metabolic comorbidities, including non-alcoholic fatty liver disease (NAFLD), type 2 diabetes mellitus (T2DM), and dyslipidemia[6]. Although pharmacological inhibition of DNL enzymes or TG synthases has demonstrated lipid-lowering potential, these approaches often lack tissue selectivity and may trigger compensatory metabolic responses, limiting therapeutic efficacy and safety[7].

Long-chain fatty acids (LCFAs) are major lipid substrates derived from dietary intake and adipose lipolysis[8]. Their conversion into long-chain fatty acyl-CoA (LCFA-CoA) is catalyzed by acyl-CoA synthetase long-chain family member 1 (ACSL1), which is markedly upregulated in mature adipocytes and adipose tissue[9-12]. This facilitates excessive esterification of LCFAs into TGs. Selective inhibition of ACSL1 in adipose tissue offers a promising strategy to limit pathological lipid accumulation while preserving systemic lipid metabolism. However, to date, few small-molecule ACSL1 inhibitors have been reported, and their pharmacological efficacy in adipocytes remains inadequately validated[13,14].

Despite its importance, the regulation of LCFA activation and TG biosynthesis in adipocytes has been relatively underexplored. Nicotinamide adenine dinucleotide (NAD^+) is a central redox coenzyme and metabolic cofactor for various NAD^+-dependent enzymes involved in energy metabolism, genome maintenance, and cellular stress responses[15,16]. In adipose tissue, NAD^+ homeostasis is primarily sustained through the nicotinamide salvage pathway, in which nicotinamide phosphoribosyltransferase (NAMPT) functions as the rate-limiting enzyme[17]. Recent studies have shown that reduced NAMPT expression and NAD^+ levels impair mitochondrial oxidative metabolism and promote lipogenesis, contributing to obesity-associated lipid dysfunction[18-20]. Thus, restoring NAD^+ biosynthesis through NAMPT activation represents a potential strategy for rebalancing adipocyte lipid metabolism. Advances in structural biology have facilitated the development of NAMPT activators with high specificity, which have shown therapeutic benefits in models of aging, cancer, neurodegeneration and other diseases[21-24]. However, their application in obesity remains underexplored.

Our previous studies identified Bouchardatine (Bou), a β-indoquinazolinone alkaloid, as a candidate metabolic modulator for diet-induced obesity (DIO)[25]. Nevertheless, Bou's limited solubility and reactive aldehyde group compromised its drug-ability. To improve upon Bou, we synthesized a series of β-indoquinazolinone derivatives using palladium oxidative addition complex (OAC) chemistry and identified compound b2b with superior efficacy and safety. In DIO mice, b2b significantly reduced body weight, adipose mass, and circulating lipid levels. Mechanistically, b2b suppressed ACSL1 expression, thereby inhibiting LCFA-CoA formation and TG biosynthesis. Using activity-based proteome profiling (ABPP), we identified NAMPT as the direct molecular target of b2b. Subsequent validation confirmed that b2b activates NAMPT and elevates intracellular NAD^+ levels to enhance NAD^+-dependent regulatory protein SIRT1 activity, leading to transcriptional repression of ACSL1. Together, these findings reveal a previously unrecognized mechanism whereby pharmacological activation of the NAMPT-NAD^+-SIRT1 axis modulates LCFA incorporation into TGs in adipose tissue. This work establishes b2b as a novel NAMPT activator with anti-lipogenic properties and highlights the potential of adipose-specific metabolic reprogramming strategies for obesity treatment.

2. Results

2.1. Structural modification of natural product bouchardatine leads to a potent lipid-lowering compound b2b

The natural product Bouchardatine (Bou), despite its anti-obesity potential, suffered from limited efficacy and aldehyde-mediated toxicity[26,27]. We therefore pursued scaffold modification *via* palladium-catalyzed oxidative addition complex (OAC) chemistry[28], generating a library of quinazolinone derivatives by C−N functionalization (Fig. 1A and Supporting Information Fig. S1)[29]. Comprehensive pharmacological screening was performed using the 3T3-L1 adipocyte model[30], a standardized assay to evaluate the effects of compounds on lipids accumulation. The results indicated that most amination derivatives, from which the aldehyde groups were removed, exhibited varying degrees of enhanced lipid-lowering activity (Fig. 1B and Supporting Information Table S1). Among these, compound b2b was identified as exceptionally potent. It exhibited markedly superior lipid-lowering activity (EC_{50} = 0.37 μmol/L) compared to Bou (EC_{50} = 22.4 μmol/L) (Fig. 1C and D), low cytotoxicity in 3T3-L1 adipocytes (CC_{50} = 31.9 μmol/L; Fig. 1E), and minimal hERG channel inhibition (IC_{50} > 50 μmol/L; Supporting Information Fig. S2A).

Mechanistically, b2b suppressed lipid accumulation throughout all stages of adipocyte differentiation, a distinct temporal effect compared to Bou's predominantly early-stage inhibition (Fig. 1F and G; Supporting Information Fig. S3). Consistent with its enhanced safety, b2b had negligible impact on cell cycle progression or apoptotic markers (Fig. 1H and I; Fig. S2B). These findings highlight b2b as a significantly more potent and safer lipid-lowering agent than Bou, suggesting a distinct and potentially novel mechanism of action underpinning its superior pharmacological profile, which prompted further investigation.

2.2. b2b attenuates diet-induced obesity and improves metabolic health in mice

Preliminary *in vivo* screening in a model C57BL/6J mice fed with a short-term (two-week) high-fat and cholesterol (HFC) diet indicated b2b's potential for weight reduction, showing

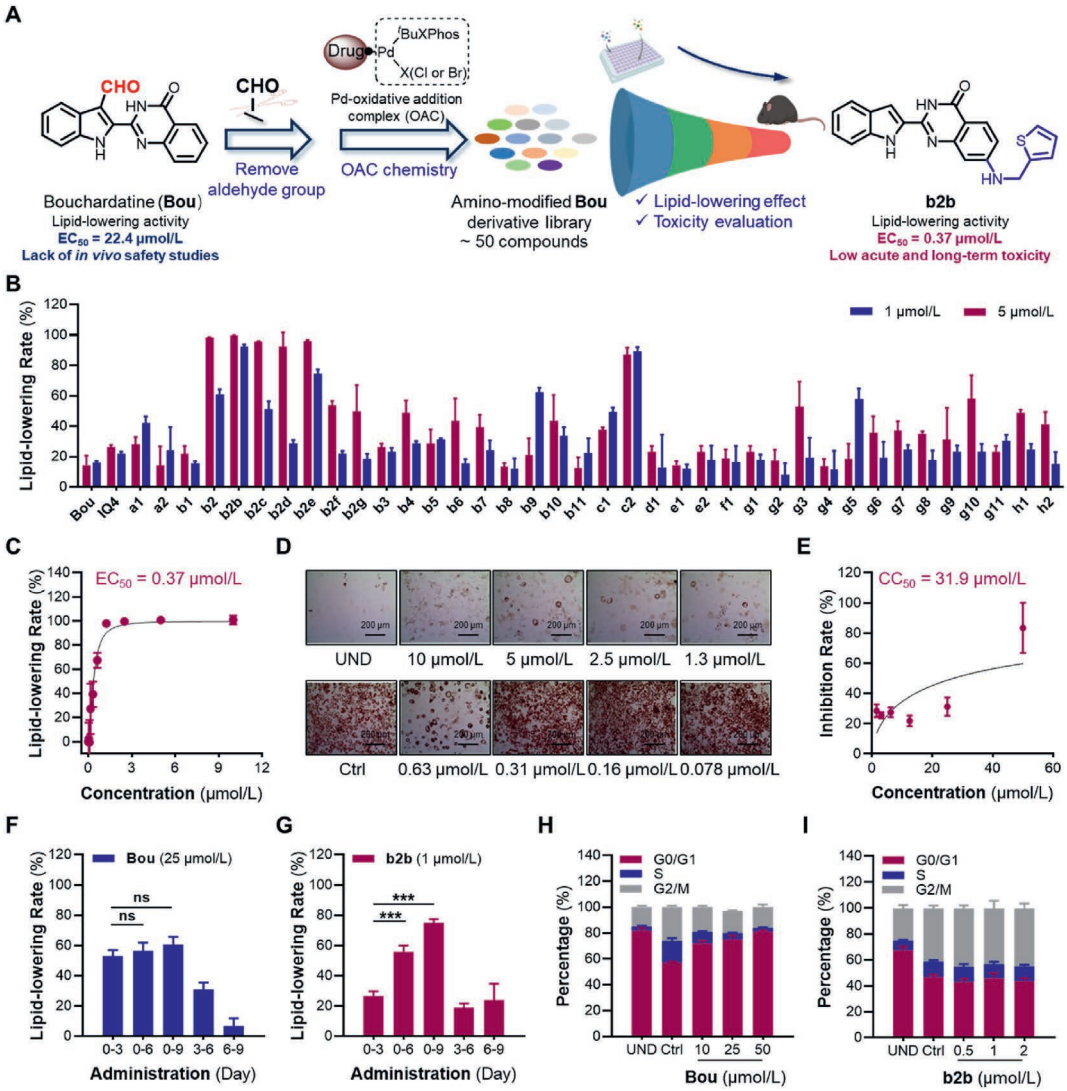

Figure 1 Discovery of compound b2b with better lipid-lowering activity from natural product Bouchardatine (Bou). (A) Schematic diagram of the discovery of b2b. (B) Preliminarily evaluation of the lipid-lowering activity of Bou derivatives at concentrations of 1 and 5 μmol/L. (C) EC_{50} of b2b for lipid-lowering activity on 3T3-L1 adipocytes. (D) Representative Oil Red O staining images of 3T3-L1 adipocytes treated with b2b. (E) The CC_{50} of 3T3-L1 adipocytes treated with b2b over 9 days. (F) Evaluation of the lipid-lowering rate of Bou at various stages of differentiation in 3T3-L1 adipocytes. (G) Evaluation of the lipid-lowering rate of b2b at various stages of differentiation in 3T3-L1 adipocytes. (H) Analysis of cell cycle in 3T3-L1 adipocytes treated with or without Bou for 24 h (I) Analysis of cell cycle in 3T3-L1 adipocytes treated with or without b2b for 24 h. Data are expressed as mean ± SD from 3 independent experiments. (ns) $P \geq 0.05$, $^{*}P < 0.05$, $^{**}P < 0.01$, $^{***}P < 0.001$ compared with different group.

dose-dependent reductions in weight gain (Fig. 2A and Supporting Information Fig. S4A) and fat accumulation (Fig. S4B), while a minimal impact on food intake (Fig. S4C). We further assessed its efficacy in a more robust diet-induced obesity (DIO) model. C57BL/6J mice fed with a HFC diet for four months developed significant obesity (35.5% greater body mass than chow-fed controls). Subsequent treatment with b2b (20 mg/kg/day, i.p.) for five weeks markedly reduced total body weight by approximately 20% with body weight stabilizing after three weeks of treatment (Fig. 2B and C). b2b treatment cause an early-stage reduction in food intake (Fig. 2D), but over time, it minimally affected food intake (Supporting Information Fig. S5A), indicating that b2b exerts an appetite-suppressive effect in the early stage of administration, which may be associated with an acute anorectic response. However, this effect gradually diminishes in the later stage, and the overall appetite-suppressive effect is not significant. b2b treatment dramatically impacted adipose tissue, reducing the weights of both epididymal (eWAT) and inguinal (iWAT) white adipose depots by approximately 60% (Fig. 2E). Histopathological analysis confirmed that b2b significantly reduced adipocyte size (Fig. 2F); meanwhile, b2b led to an increase in adiponectin levels (Fig. 2G and Fig. S5B) and a decrease in the levels of inflammatory factors (*e.g.*, IL-6, TNFα) in adipose tissue (Fig. S5C), indicating amelioration of obesity-induced adipocyte hypertrophy and dysfunction[31]. In addition, b2b improved liver function, as supported by reduced accumulation of lipid droplet in hepatocytes (Fig. 2H and Fig. S5D), and decreased levels of circulating liver injury markers AST and ALT (Fig. S5E)[32]. Moreover, b2b ameliorated obesity-induced impaired glucose tolerance (Fig. 2I and Fig. S5F), while

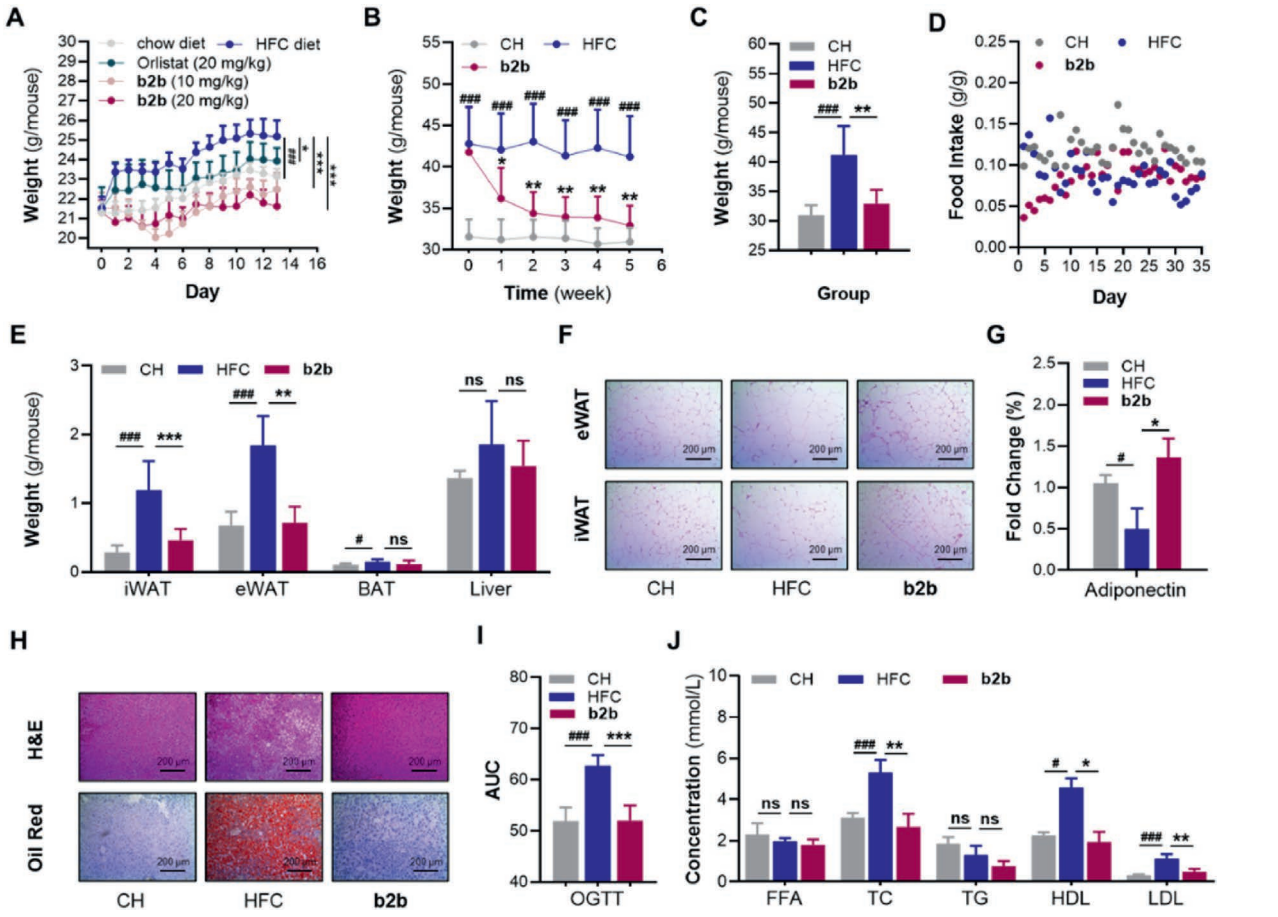

Figure 2 Amelioration of HFC feeding induced obesity and metabolic disorders by compound b2b. (A) Preliminary evaluation of weight loss efficacy of orlistat and b2b on a model that C57BL/6J mice fed a short-term HFC diet. Average weight of mice during two weeks of drug treatment. (B−J) C57BL/6J mice were fed with a HFC diet for 4 mouths, and b2b was administered for the nest 5 weeks at a dose of 20 mg/kg every day by i.p. CH group: mice were fed with a chow diet. HFC group: mice were fed with a high-fat diet containing 1% cholesterol and treated with solvent every day by i.p. After treatment, mice were anesthetized, plasma and tissues studied were isolated and weighted, and the chemicals in plasma were determined. (B) Weight of mice during the five-week administration cycle. (C) Weight of mice after the five-week administration cycle. (D) Daily food intake during the five-week administration cycle. (E) Weight of fat mass and liver after the five-week administration cycle. (F) Representative microscopy images of the fat mass after H&E staining. (G) Adiponectin levels in eWAT. Data were expressed as mean ± SD from 3 mice for each group. (H) Representative microscopy images of the liver after H&E or Oil Red O staining. (I) The AUC of OGTT. (J) Chronic effects of b2b on metabolic parameters. Data are expressed as mean ± SD from 4 mice for each group. Other data were expressed as mean ± SD from 6 mice for each group. (ns) $P \geq 0.05$, $^{\#}P < 0.05$, $^{\#\#}P < 0.01$, $^{\#\#\#}P < 0.001$ compared with CH group, (ns) $P \geq 0.05$, $^{*}P < 0.05$, $^{**}P < 0.01$, $^{***}P < 0.001$ compared with HFC group.

reducing serum glucose levels (Fig. S5G), triglycerides, and low-density lipoprotein cholesterol (LDL-C) (Fig. 2J) yet no significant changes in adiponectin and leptin levels (Fig. S5H and S5I). Together, b2b partially reversed obesity-induced metabolic disorders. These results indicated that b2b was a promising anti-obesity compound.

Additionally, b2b exhibited a favorable acute safety profile, with a maximum tolerated dose exceeding 500 mg/kg in mice (Supporting Information Table S2). Chronic administration (one-month) resulted in negligible changes in body weight and water intake (Supporting Information Fig. S6A and S6B), but a slight reduction on food intake (Fig. S6C). Consistent with its favorable safety profile, b2b did not induce significant morphological changes in organ tissues, indicating its favorable *in vivo* safety (Fig. S5J). While b2b adheres to Lipinski's rules *in silico* (Supporting Information Table S3), its pharmacokinetic profile revealed rapid systemic clearance ($t_{1/2} < 1$ h) and low bioavailability ($F_{0-\infty} < 10\%$) (Supporting Information Table S4), which suggested the need for formulation optimization for therapeutic application.

Collectively, these findings establish that b2b possesses potent anti-obesity effects, significantly reduces adiposity, and ameliorates associated metabolic comorbidities *in vivo*.

2.3. b2b disrupts LCFA flux and triglyceride biosynthesis by inhibiting ACSL1 in adipocytes

Given its pronounced anti-obesity effects, we next investigated the underlying lipid-lowering mechanisms of b2b. Proteomic profiling indicated that the differentially expressed proteins were primarily enriched in the fatty acid metabolic process (Fig. 3A). Gene Ontology (GO) analysis highlighted ACSL1 as a significantly downregulated protein involved in fatty acid anabolism (Fig. 3B).

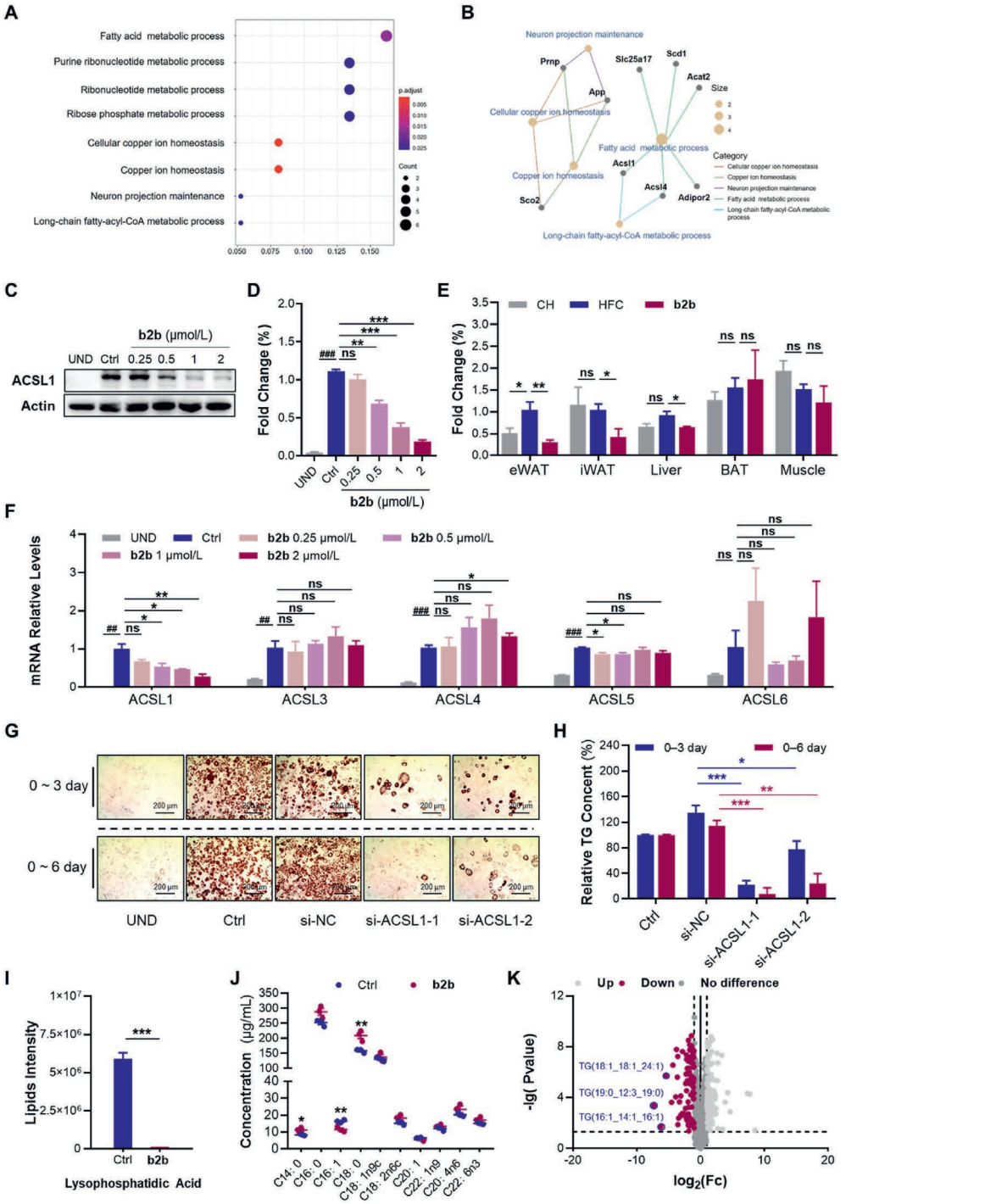

Figure 3 Compound b2b reduced the accumulation of triglycerides in 3T3-L1 adipocytes by inhibiting the expression of ACSL1. (A, B) Gene ontology (GO) analysis and the main differential proteins. The 3T3-L1 adipocytes were treated with or without 1 μmol/L b2b for 3 days and then harvested for proteomics analysis. (C, D) The protein levels of ACSL1 in 3T3-L1 adipocytes treated with b2b for 3 days. (E) Analysis of ACSL1 protein levels in different tissues of mice. (F) The mRNA levels of ACSL1 in 3T3-L1 adipocytes treated with b2b for 3 days. (G) Representative Oil Red O staining images of normal or ACSL1-knockdown 3T3-L1 adipocytes. (H) Relative TG content of normal or ACSL1-knockdown 3T3-L1 adipocytes. (I) The lipid intensity of intracellular lysophosphatidic acid in 3T3-L1 adipocytes treated with b2b for 3 days. (J) Metabolomics targeting LCFAs of 3T3-L1 adipocytes treated with or without 1 μmol/L b2b for 3 days. (K) Volcano of metabolomics for lipids of 3T3-L1 adipocytes treated with or without 1 μmol/L b2b for 3 days. Data are expressed as mean ± SEM from 3 independent experiments. (ns) $P \geq 0.05$, $^{\#}P < 0.05$, $^{\#\#}P < 0.01$, $^{\#\#\#}P < 0.001$ or $^{*}P < 0.05$, $^{**}P < 0.01$, $^{***}P < 0.001$ compared with Ctrl group.

While ACSL4 was also identified, b2b treatment did not induce lipid peroxidation (Supporting Information Fig. S7A) or activate ferroptosis-related biomarkers (Fig. S7B)[33].

It was found that ACSL1 expression increased progressively during 3T3-L1 adipocyte differentiation (Supporting Information Fig. S8A and S8B), and b2b dose-dependently suppressed ACSL1 at both protein and transcriptional levels in 3T3-L1 adipocytes (Fig. 3C, D and Fig. S8C). This downregulation was also observed *in vivo*, where b2b treatment markedly reduced ACSL1 expression in eWAT and iWAT, with a modest reduction in liver tissues of DIO mice, but exerted minor effects on BAT and skeletal muscle (Fig. 3E and Fig. S8D). Furthermore, b2b also exhibited a certain degree of cell selectivity, and exerted minor effects on ACSL1 in other cells (*e.g.*, HepG2, C2C12, and SH-SY5Y cell) (Fig. S8E). Notably, b2b exhibited selectivity for inhibiting ACSL1 over other ACSL isoforms tested (Fig. 3F). ACSL1 knockdown in 3T3-L1 adipocytes resulted in a significant reduction in lipid accumulation, and this decrease became more pronounced with the extension of knockdown duration and the reduction of ACSL1 expression levels (Fig. 3G, H and Fig. S8F).

ACSL1 is highly expressed in adipose and liver tissue[11,12]. This protein catalyzes the formation of LC acyl-CoA from LCFAs of different sources in the endoplasmic reticulum, a critical step for their incorporation into TGs (Fig. S8G). To determine if b2b impairs this process, we analyzed lipid profiles. Untargeted lipidomic analysis showed that b2b treatment significantly reduced levels of lysophosphatidic acid (LPA), an early intermediate in TG biosynthesis downstream of LCFA-CoA formation (Fig. 3I). Targeted metabolomics further revealed that b2b resulted in the intracellular accumulation of unconjugated LCFAs, including myristic acid and stearic acid (Fig. 3J). These suggested that b2b-induced inhibition of ACSL1 leads to impaired LCFA activation, causing intracellular accumulation of LCFAs and reduced LPA level. Consequently, b2b treatment reduced the content of most LCFAs-based TGs in adipocytes (Fig. 3K). These results demonstrated the selective pharmacological effect of b2b in disrupting LCFA flux toward TG biosynthesis.

These results show that compound b2b inhibits LCFA activation by selectively downregulating ACSL1 expression, thereby impairing TG biosynthesis in adipocytes.

2.4. *Identification of compound b2b as NAMPT activator in 3T3-L1 adipocytes*

Leveraging active photoaffinity labeling-based chemoproteomics[34], we explored the targets of b2b in 3T3-L1 adipocytes. A photoreactive probe (P1) was designed by incorporating a diazirine electrophilic warhead into the b2b scaffold (Supporting Information Fig. S9A), which retained lipid-lowering efficacy in 3T3-L1 adipocytes (EC_{50} = 13.7 μmol/L) (Fig. S9B and S9C) and preserved its ACSL1 inhibitory activity (Fig. S9D). Following the chemoproteomic workflow (Fig. 4A), UV-induced crosslinking of P1 to its protein targets resulted in the formation of adducts, which were subsequently tagged with biotin *via* copper-catalyzed azide-alkyne cycloaddition. These biotinylated adducts were enriched using streptavidin and ensured technically feasible (Fig. 4B), followed by LC−MS/MS-based proteomic analysis. Pathway-centric analysis of the captured proteins revealed NAMPT, a key enzyme in fatty acid metabolism, as the potential target of b2b (Fig. 4C). Pulldown assays confirmed that P1 formed covalent adducts with recombinant NAMPT, and this interaction was effectively disrupted by pre-treatment with b2b, both in adipocyte lysates and in recombinant NAMPT (Fig. 4D). Cellular thermal shift assay (CESTA) demonstrated an increased thermal stability of NAMPT in b2b-treated adipocyte lysates (Fig. 4E and Supporting Information Fig. S10A), suggesting direct intracellular interactions. Surface plasmon resonance (SPR) confirmed that b2b binds to NAMPT with a dissociation constant (K_D) of 0.78 μmol/L (Fig. 4F and Fig. S10B−S10D). Collectively, these results confirmed that b2b targets NAMPT in adipocytes.

Subsequent to target engagement confirmation, we investigated the functional modulation of adipocyte NAMPT by b2b. Quantitative enzymatic assays demonstrated dose-dependent activation of NAMPT by b2b, positioning b2b as a novel NAMPT activator (Fig. 4G). Photolabeling coupled mass spectrometric foot-printing using P1 investigated the binding site of b2b on NAMPT (Supporting Information Fig. S11A). Structural alignment with NAT (reported as a NAMPT activator) co-crystallized complexes[21] indicated that the amino acid residues labeled by P1 were in proximity to the NAT binding pocket, suggesting that P1 might interact with NAMPT at this location (Fig. S11B−S11D). The predicted binding site of b2b also colocalized with the NAT binding site and the residues labeled by P1, leading us to hypothesize that the binding site of b2b on NAMPT is similar to that of NAT. To verify this hypothesis, we constructed mutant proteins with key amino acid mutations near the NAT pocket (V242-P273-I309) and those potentially interacting with b2b (Y188-Y240-Q305) (Fig. S11E and S11F). *In vitro* enzyme activity assay demonstrated that the agonistic activity of b2b on these two mutant proteins was diminished, suggesting that b2b may bind near the NAT pocket (Fig. S11G). Molecular dynamics simulations further revealed that the quinazolinone core of b2b engages with substrate-binding subpockets, while maintaining partial solvent exposure, which distinguishes it from deep catalytic site binders (Fig. 4H). These findings suggested that b2b is an activator of NAMPT in adipocytes, likely exerting its effect by binding near the NAT binding pocket of NAMPT.

Together, these results indicated that compound b2b targets adipocyte NAMPT and functions as an activator, thereby increasing intracellular NAD^+ levels.

2.5. *NAMPT-NAD^+-SIRT1 axis mediates b2b's regulation of triglyceride biosynthesis by inhibiting ACSL1 in adipocytes*

To investigate the pharmacological regulatory effect of NAMPT on TG biosynthesis, we generated NAMPT-knockdown (NAMPT-KD) 3T3-L1 adipocyte models using siRNA-mediated silencing (Supporting Information Fig. S12A). Triglyceride levels were decreased in NAMPT-KD adipocytes, which may be associated with that NAD^+ is important for energy metabolism[35]. However, it is noteworthy that the anti-lipid accumulation effect of b2b was diminished in NAMPT-KD adipocytes, while administration of NMN (the direct precursor of NAD^+) to NAMPT-KD adipocytes led to a significant reduction in lipid accumulation. These results confirming the NAMPT-dependent nature of its anti-lipid accumulation action (Fig. 5A and B). In addition, although NAMPT is upregulated during the differentiation of 3T3-L1 adipocytes, b2b exerted a minimal effect on the protein level of NAMPT during adipocyte differentiation (Fig. S12B and S12C). Considering the abundance and functional output of NAMPT are not equivalent, anti-lipid accumulation effect of b2b was primarily driven by functional enhancement rather than alterations in target abundance.

Although ACSL1 plays a key role in the incorporation of LCFAs into TGs, the upstream regulatory mechanisms controlling

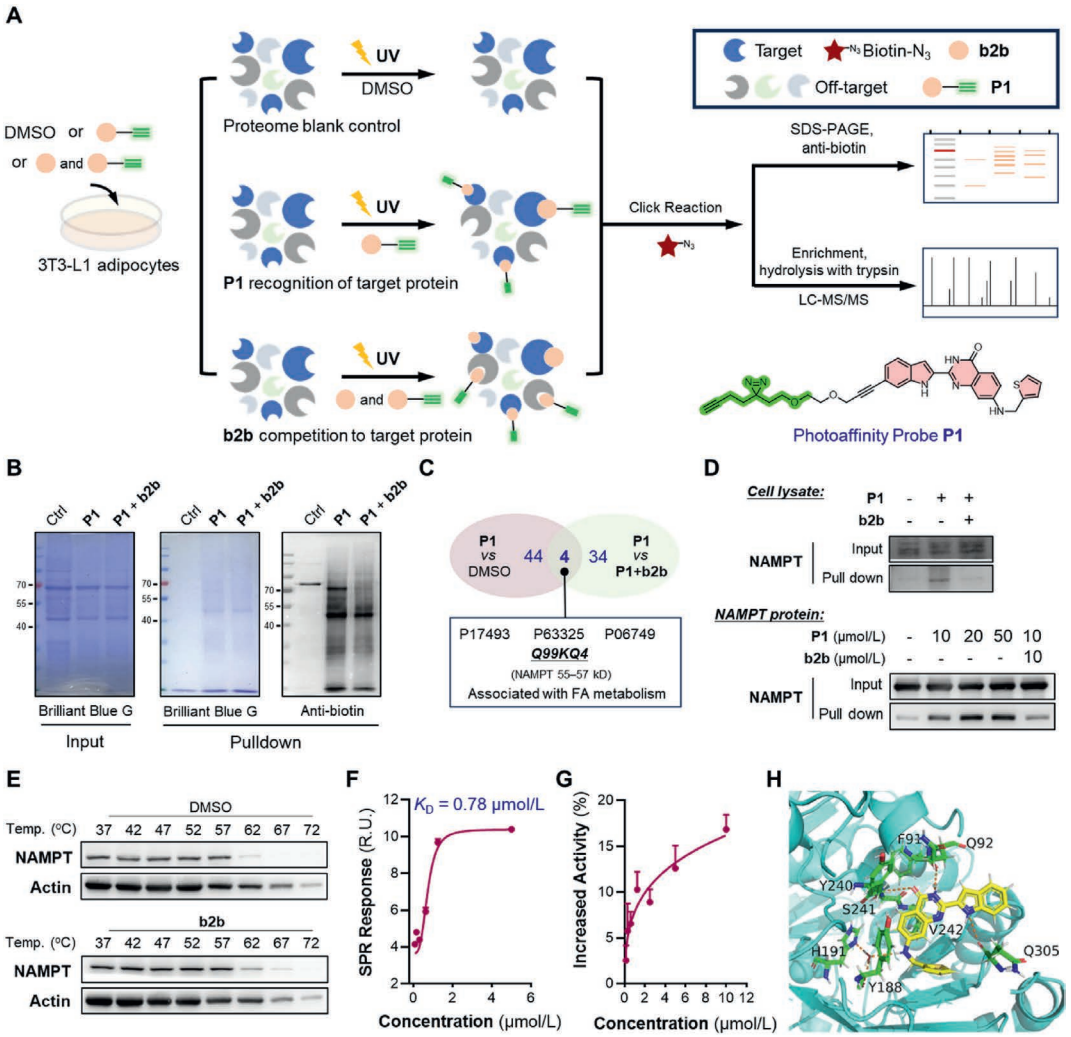

Figure 4 Compound b2b targeted NAMPT as an activator in 3T3-L1 adipocytes. (A) Schematic diagram of intracellular photoaffinity probe for target discovery. (B) Protein chromogenic reaction results of cell lysates incubated by different groups after covalent cross-linking, clicking reaction and streptavidin incubation and elution. 3T3-L1 adipocytes were treated with DMSO (Ctrl), P1 (15 μmol/L) or P1 (15 μmol/L) and b2b (15 μmol/L) for 2.5 h and then harvested for analysis of intracellular targets. (C) Retrieval process of potential targets of b2b. (D) Intracellular and extracellular pull down of NAMPT. Intracellular samples were 3T3-L1 adipocytes treated with DMSO, P1 (15 μmol/L) or P1 (15 μmol/L) and b2b (15 μmol/L) for 2.5 h. Extracellular samples were purified NAMPT. (E) CETSA analysis of thermal stability of b2b to NAMPT in 3T3-L1 adipocytes. The samples were 3T3-L1 adipocytes treated with or without b2b (10 μmol/L). (F) Analysis of binding affinity between b2b and NAMPT by SPR assay. (G) NMN trapping experiment for evaluation of influence on NAMPT activity of b2b. (H) Analysis of binding mode between b2b and NAMPT (PDB: 7ENQ). The predicted ΔG was −23.03 kcal/mol (ΔG of NAT is −36.6 kcal/mol). Data were expressed as mean ± SD from 3 independent experiments. (ns)$P \geq 0.05$, *$P < 0.05$, **$P < 0.01$, ***$P < 0.001$ compared with Ctrl group.

its expression remain a significant gap in adipocyte biology. Treatment with si-NAMPT attenuated b2b-mediated suppression of ACSL1 expression and supplementation of NMN can restore the inhibition of ACSL1 both at the protein and transcriptional levels (Fig. 5C and D), suggesting a potential regulatory mechanism through which NAMPT influence ACSL1 expression. NAMPT is the most critical enzyme for maintaining intracellular NAD^+ levels. Compound b2b could increase cellular NAD^+ levels (Fig. 5E), and analysis of NAD^+ and ACSL1 levels in adipose tissue from b2b-treated obese mice revealed a negative correlation between NAD^+ and ACSL1 levels (Fig. 5F and G). In addition, both NMN and NAT could reduce lipid accumulation (Supporting Information Fig. S13A and S13B) and downregulate ACSL1 expression (Fig. 5H and I). We further measured the intracellular levels of several LCFAs in NAT-treated 3T3-L1 adipocytes, and found that NAT also increased the levels of most LCFAs, which was consistent with its inhibitory effect on ACSL1 (Fig. 5J). Increased NAD^+ levels can enhance the activity of NAD^+-dependent enzymes. As a vital NAD^+-dependent enzyme, SIRT1 has been reported to be extensively involved in metabolic regulation[36,37]. We aim to further investigate whether activation of NAMPT downregulates the expression of ACSL1 *via* SIRT1. We constructed SIRT1-knockdown (SIRT1-KD) 3T3-L1 adipocytes (Supporting Information Fig. S14). SIRT1-KD did not significantly alter intracellular triglyceride levels (Fig. 5K); however, the anti-lipid accumulation effect of b2b was largely abrogated (Fig. 5L), as was its regulatory capacity to inhibit ACSL1 at both the protein and transcriptional levels (Fig. 5M and N).

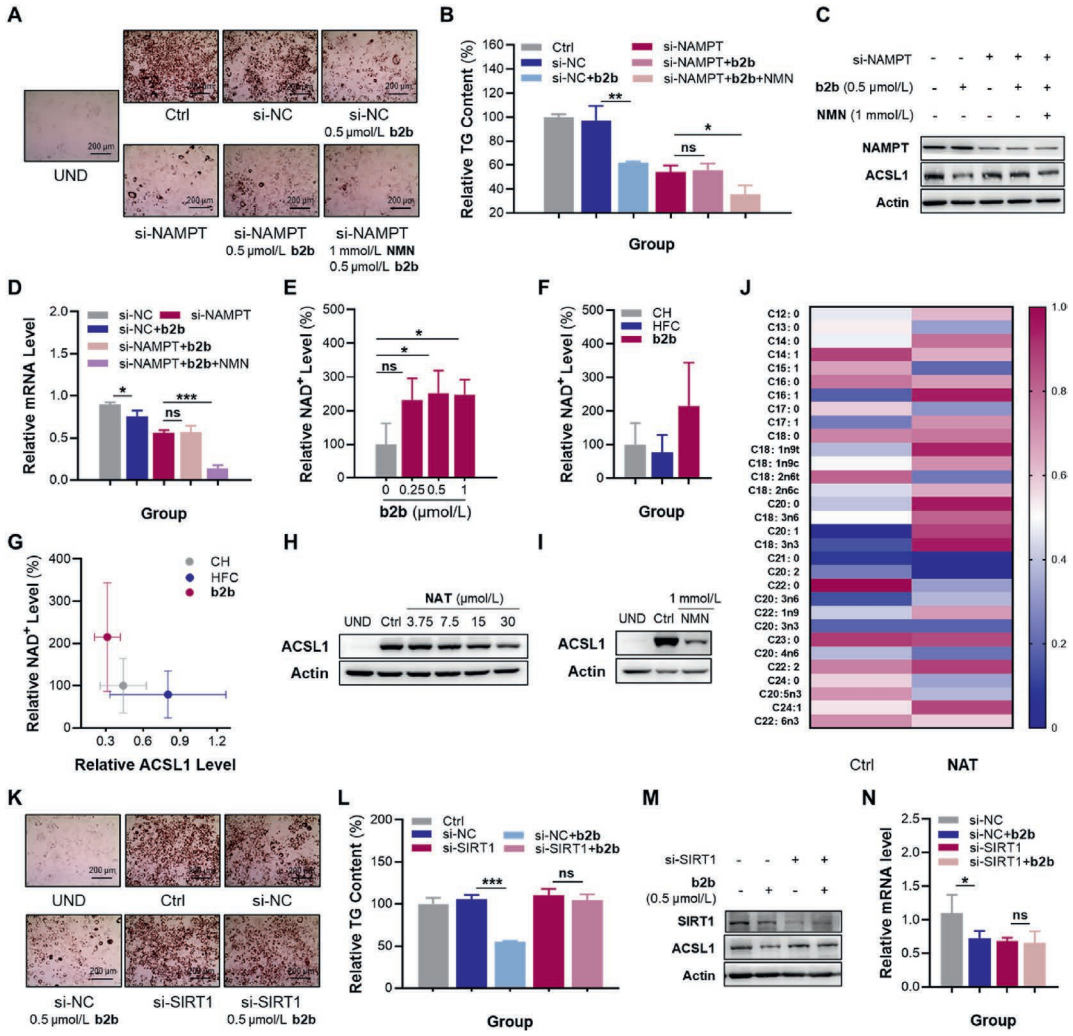

Figure 5 Compound b2b inhibited TG biosynthesis by regulating ACSL1 expression through NAMPT-NAD$^+$-SIRT1 axis. (A) Representative pictures of Oil Red O staining of normal or NAMPT-knockdown 3T3-L1 adipocytes. (B) Relative TG content of normal or NAMPT-knockdown 3T3-L1 adipocytes treated with or without b2b (0.5 μmol/L) or NMN (1 mmol/L). (C) The protein levels of ACSL1 in normal or NAMPT-knockdown 3T3-L1 adipocytes treated with or without b2b or NMN. (D) The mRNA levels of ACSL1 in normal or NAMPT-knockdown 3T3-L1 adipocytes treated with or without b2b or NMN. (E) The relative NAD$^+$ level of 3T3-L1 adipocytes treated with or without b2b. (F) The relative NAD$^+$ level of eWAT of mice. (G) The relationship between the relative NAD$^+$ level and the relative ACSL1 level in eWAT of mice. (H) The protein levels of ACSL1 in 3T3-L1 adipocytes treated with or without NAT for 3 days. (I) The protein levels of ACSL1 in 3T3-L1 adipocytes treated with or without NMN for 3 days. (J) The results of targeted LCFA metabolomics within 3T3-L1 adipocytes treated with or without NAT (10 μmol/L) for 3 days. (K) Representative pictures of Oil Red O staining of normal or SIRT1-knockdown 3T3-L1 adipocytes. (L) Relative TG content of normal or SIRT1-knockdown 3T3-L1 adipocytes treated with or without b2b (0.5 μmol/L). (M) The protein levels of ACSL1 in normal or SIRT1-knockdown 3T3-L1 adipocytes treated with or without b2b. (N) The mRNA levels of ACSL1 in normal or SIRT1-knockdown 3T3-L1 adipocytes treated with or without b2b. Data are expressed as mean ± SD from 3 independent experiments. (ns)$P \geq 0.05$, *$P < 0.05$, **$P < 0.01$, ***$P < 0.001$ compared with Ctrl group.

These results indicate that the NAMPT-NAD$^+$-SIRT1 axis serves as a negative regulatory axis for ACSL1 in adipocytes, and b2b exerts inhibitory regulation on ACSL1 by activating the NAMPT-NAD$^+$-SIRT1 axis, thereby reducing lipid accumulation in adipose tissue.

3. Discussion

The escalating global obesity epidemic necessitates novel therapeutic strategies beyond current interventions, which often have limited long-term efficacy or target appetite centrally[38-40]. This study introduces b2b, a rationally designed β-indoquinazolinone derivative, as a potent anti-obesity agent. Compound b2b exerts its anti-lipid accumulation effect not by inhibiting the early stage of adipogenesis, but mainly by acting on the late stage of lipid synthesis where fatty acids are converted into triglycerides. It could reduce body weight in DIO mice, improve the functions of adipose and hepatic tissues, and ameliorate systemic metabolic disorders. In toxicity studies at the cellular and animal levels, b2b also showed favorable safety profiles, which serves as an important foundation for developing therapeutic molecules against chronic obesity. However, it should be pointed out that b2b

exhibits poor pharmacokinetic properties, characterized by a short half-life and low oral bioavailability, which may hinder its applicability in clinical settings. Future studies should prioritize improving the drug-likeness of b2b, which can be achieved by systematic structure-pharmacokinetic relationship studies combined with rational structural optimization in medicinal chemistry or lipids and lipid-based formulations to optimize its pharmacokinetic properties[41,42].

A significant finding is the elucidation of the NAMPT-NAD^+-SIRT1 axis as a previously unrecognized regulatory axis for ACSL1 in adipocytes, and b2b can activate NAMPT and elevate intracellular NAD^+ levels to enhance NAD^+-dependent regulatory protein SIRT1 activity, leading to transcriptional repression of ACSL1, which ultimately curtails the incorporation of LCFAs into TGs, a key process in adipocyte lipid accumulation. While NAMPT activation or NAD^+ repletion is explored for various age-related and metabolic conditions[43-46], their direct linkage to the control of LCFA esterification *via* ACSL1 modulation in adipocytes for obesity treatment is novel. Our findings provide new insights and perspectives into understanding the regulatory role of the NAMPT-NAD^+-SIRT1 axis in triglyceride synthesis in adipose tissue, as well as achieving the inhibitory regulation of ACSL1.

In addition, b2b exhibited a weaker impact on key enzymes of glucose and lipid metabolism or DNL compared to its effect on inhibition of LCFA activation *via* ACSL1 (Supporting Information Fig. S15). This selectivity is crucial, since we observed that obesity did not induce an increase in the expression of enzymes related to lipogenesis (Supporting Information Fig. S16)[47]. Current studies have identified the contribution of ACSL1 to β-oxidation[48]. From our results, inhibiting ACSL1 by b2b does not have significant effects on mitochondrial aerobic respiration in 3T3-L1 adipocytes (Supporting Information Fig. S17A) and the expression of carnitine palmitoyltransferase 1β (CPT1β), the rate-limiting enzyme of the β-oxidation pathway (Fig. S17B). Furthermore, b2b exhibits a certain degree of cellular and tissue selectivity in its inhibitory regulation of ACSL1, exerting a more pronounced inhibitory effect on ACSL1 levels in adipocytes and adipose tissue. Notably, we did not observe elevated serum FFAs or ectopic lipid deposition in major organs associated with ACSL1 inhibition. This suggests that in this context, the primary impact of ACSL1 modulation by b2b is on TG storage. b2b can significantly reduce hepatic TG accumulation while decreasing ACSL1 expression. However, the regulatory role of ACSL1 in hepatic lipid metabolism is more complex, which warrant further investigation[49-51].

We identified b2b as a novel activator of NAMPT. Although the activation capacity of b2b was weaker than the well-established activator NAT *in vitro*, it significantly elevated intracellular NAD^+ levels, suggesting that b2b possesses a favorable potential for NAMPT activation within cells. Furthermore, we evaluated the effects of representative NAMPT activators on NAD^+ levels in adipocytes. The results showed that both NAT and compound **60** effectively activated NAMPT and increased intracellular NAD^+ levels, consistent with their lipid-lowering properties, while compound SBI-797812 was comparatively weaker and its lipid-lowering activity was less pronounced (Supporting Information Fig. S18)[22,52].

Previous studies have established the pivotal role of the NAMPT-NAD^+-SIRT1 axis in regulating brown adipose tissue function and thermogenesis[53-55]. Our results demonstrate that b2b can upregulate the levels of key brown adipogenic proteins UCP1 and PGC-1α, but the effect was not pronounced at its pharmacologically effective concentrations (Supporting Information Fig. S19). Notably, our study is the first to demonstrate that NAMPT signaling activation inhibits TG biosynthesis and metabolism in white adipose tissue by transcriptionally regulating ACSL1, thereby enhancing the understanding of NAMPT' role in energy metabolism. While PPARγ and C/EBPα have been reported to be associated with the regulation of ACSL1 levels[56,57], our results demonstrate that b2b exerts a minimal effect on their levels (Supporting Information Fig. S20), suggesting an alternative regulatory route. The precise molecular details of how SIRT1, an NAD^+-dependent deacetylase, represses ACSL1 transcription remain a key area for our future exploration. Although the effects of b2b administration on the NAMPT-NAD^+-SIRT1 axis *in vivo* are of great interest, the complexities of validating this in animal models currently limit our ability to address this aspect within the scope of the present study. However, we measured NAMPT levels in various tissues of DIO mice treated with b2b (Supporting Information Fig. S21). Obesity induced a reduction in NAMPT levels in adipose and hepatic tissues, and activating NAMPT still holds positive exploratory significance for the treatment of obesity.

4. Conclusions

In conclusion, we have identified a novel NAMPT activator, b2b, that ameliorates obesity by inhibiting adipocyte ACSL1 expression through NAMPT−NAD^+−SIRT1 axis signaling pathway. This work uncovers a new druggable axis for the targeted treatment of obesity and provides a valuable pharmacological tool and lead compound for further development.

5. Experimental

5.1. Chemistry synthesis

All chemicals were of reagent grade quality or better, obtained from commercial suppliers, and used without further purification. Column chromatography was conducted on silica gel (200−300 mesh) from Shanghai Titan Scientific Co., Ltd. TLC (HSGF 254) from Yantai Jiangyou Silica Gel Development Co. Ltd (Yantai, China) was used for monitoring the reaction process. All the key intermediates and products were determined by using ^{1}H NMR and ^{13}C NMR recorded in a Bruker BioSpin GmbH spectrometer (^{1}H at 400 or 500 MHz, ^{13}C at 100 or 125 MHz), and chemical shifts were reported in parts per million using the residual solvent peaks as internal standards ($CDCl_3$ = 7.26 ppm for ^{1}H NMR and 77.16 ppm for ^{13}C NMR, CD_3SOCD_3 = 2.50 ppm for ^{1}H NMR and 39.6 ppm for ^{13}C NMR, CD_3OD = 4.87 and 3.31 ppm for ^{1}H NMR, and 49.17 ppm for ^{13}C NMR). All the target products were also determined by using a Shimadzu LCMS-IT-TOF instrument with an ESI-ACPI mass selective detector. Flash column chromatography was performed with silica gel (200−300 mesh). The purities of the synthesized compounds were confirmed to be higher than 95% using analytical HPLC performed with a Shimadzu LC-20AB system equipped with an AnalaRic-C18 column (4.6 mm × 250 mm, 5 μm) and eluted with methanol/water containing 0.1% TFA at a flow rate of 0.5 mL/min. The characterization information of derivatives could be found in the Supporting Information−Characterization information of the final compounds section.

5.2. Cell lines and cell culture

3T3-L1 preadipocytes (Procell), HepG2 cells and C2C12 cells were maintained in Dulbecco's Modified Eagle Medium (DMEM, Gibco, USA) supplemented with 10% fetal bovine serum (FBS, Gibco, USA) and 0.2% mycoplasma removal agent (Beyotime, China) in a humidified atmosphere at 37 °C with 5% CO_2. SH-SY5Y cells were maintained in Modified Eagle Medium/Nutrient Mixture F-12 (MEM/F12, Procell, China) supplemented with 10% fetal bovine serum and 0.1% mycoplasma removal agent in a humidified atmosphere at 37 °C with 5% CO_2.

5.3. 3T3-L1 preadipocyte differentiation assay

The differentiation of 3T3-L1 preadipocytes was conducted following a previously described protocol with modifications[58]. Two days post-confluence, the culture medium was replaced with a differentiation induction medium comprising 0.5 mmol/L 3-isobutyl-1-methylxanthine (IBMX, Sigma, USA), 1 μmol/L dexamethasone (Dex, MP, USA) and 10 μg/mL insulin (Sigma, USA) in DMEM with 10% (*v*/*v*) FBS and 0.2% (*v*/*v*) mycoplasma removal agent (Beyotime, China) for three days (Day 3). Subsequently, the medium was exchanged for DMEM containing 10% FBS, 10 μg/mL insulin, and 0.2% (*v*/*v*) mycoplasma removal agent for an additional three days (Day 6). Finally, the medium was replaced with DMEM containing and 0.2% (*v*/*v*) mycoplasma removal agent for a further three days (Day 9). The undifferentiated control group (UND group) was cultured in DMEM with normal 10% FBS and 0.2% (*v*/*v*) mycoplasma removal agent for the entire nine-day period. Stock solutions of the test compounds were prepared and stored at −20 °C. Test compounds were added to the differentiation induction medium on day 0 for three days, followed by replacement on Day 4 in the subsequent differentiation medium for another three days, and finally on Day 7 in the normal medium for another three days. The UND group and the differentiation control group received equivalent volumes of DMSO as a vehicle control throughout all experiments.

5.4. Oil red O staining assay

Oil Red O staining was performed as follows: Cells were fixed with 4% formaldehyde (*v*/*v*) for 30 min at room temperature, followed by washes with distilled water and 60% isopropanol (*v*/*v*) once each. The cells were then stained with freshly prepared Oil Red O working solution for 30 min at room temperature and washed three times with 60% isopropanol (*v*/*v*). The Oil Red O working solution was prepared by mixing 6 mL of 0.5% Oil Red O (*w*/*v*, Sigma) in isopropanol with 4 mL of ddH_2O, followed by filtration through a 0.22 μm filter (Millipore). Lipid content was quantified by extracting the Oil Red O from stained cells using 100% isopropyl alcohol and measuring optical density at 510 nm with a microplate reader (Biotek, USA).

5.5. Cell toxicity assay

The cytotoxicity of the compounds was evaluated using the Sulforhodamine B (SRB) assay. Briefly, the 3T3-L1 preadipocytes were seeded in 96-wells plates at a density of 5×10^3 cells per well in 100 μL of 10% FBS/DMEM medium and incubated until confluence. Subsequently, cells were treated with the indicated concentrations of the compounds for 9 days in a 10% FBS/DMEM medium or differentiation induction medium. Following treatment, cells were fixed with 10% trichloroacetic acid (TCA) for 30 min at room temperature, then washed three times with distilled water. Cells were stained with SRB working solution for 30 min at room temperature and washed three times with 5% acetic acid (*v*/*v*). The Sulforhodamine B (SRB) working solution was prepared by dissolving 0.4 g of Sulforhodamine B in 100 mL of 5% acetic acid (*v*/*v*). Cell viability was assessed by extracting the SRB from stained cells with 50 μL 10 mmol/L Tris and measuring the optical density at 515 nm using a microplate reader (Biotek, USA).

5.6. Cell cycle analysis

Cell cycle analysis was performed using the ImageXpress MicroConfocol (Molecular Devices, USA). 3T3-L1 preadipocytes were seeded in 96-well plates at a density of 5×10^3 cells per well in 100 μL of 10% FBS/DMEM medium and incubated until confluence. Cells were then treated with the indicated concentrations of the compounds for 24 h, fixed with 100 μL 70% ethyl alcohol (*v*/*v*) per well overnight at −20 °C, and washed three times with 100 μL of PBS (pH 7.4). Subsequently, cells were stained with 50 μL 0.5 μg/mL 4′,6-diamidino-2-phenylindole (DAPI) in PBS for 15 min at 37 °C. Cell cycle analysis was conducted using the ImageXpress MicroConfocol system and analyzed with ImageXpress software by quantifying DAPI intensity, which represents the DNA content in individual cells.

5.7. Western blotting

Cultured 3T3-L1 adipocytes were washed with PBS (pH 7.4) and collected by centrifugation at 3000×*g* for 5 min. The cells were lysed on ice for 30 min using a lysis buffer comprising 1 × RIPA lysate, 1 × protease inhibitor cocktail for general use (Beyotime), and 1 × protein phosphatase inhibitor (Solarbio). The lysates were then centrifuged at 12,000×*g* for 15 min at 4 °C to remove cellular debris. Protein concentrations were determined using a BCA protein assay kit and denatured in an SDS-PAGE Sample Loading Buffer. The protein samples were separated by SDS-PAGE and transferred onto polyvinylidene difluoride (PVDF) membranes (Millipore). Membranes were blocked with 5% (*w*/*v*) bovine serum albumin in Tris-buffered saline containing 0.1% (*v*/*v*) Tween 20 (TBST) for 1 h and incubated with primary antibodies for 16 h at 4 °C. The primary antibodies included Actin (Affinity, Cat#T0022), PPARγ (Cell Signaling Technology, Cat#2435), ACC (Cell Signaling Technology, Cat#3662), FAS (Affinity, Cat#DF6106), ACSL1 (Proteintech, Cat#13989-1-AP), NAMPT (Affinity, Cat#AF3423), SIRT1 (Affinity, Cat#DF6033), Adiponectin (Proteintech, Cat#21613-1-AP), Leptin (Proteintech, Cat#83655-3-RR). Following four washes with TBST, membranes were incubated with horseradish peroxidase-conjugated anti-mouse or anti-rabbit IgG for 1 h at room temperature. Immunoreactive signals were detected and quantified using ImageJ software.

5.8. Animal studies

The animal studies evaluating the effects of compounds on mice with a high-fat diet containing 1% cholesterol (HFC) feeding could be divided in two independent experiments, which are preliminary evaluation of weight loss effects of compounds on mice with a HFC diet and the effects of anti-obesity of compound b2b on diet-induced-obese (DIO) mice. The preliminary evaluation of the weight loss effects of compounds on HFC-fed mice was conducted followed by the produces[59]: Male C57BL/6J mice (4−6

weeks old, Guangdong Medical Laboratory Animal Center) were housed at under controlled conditions (22 ± 1 °C, 12 h light/dark cycle) with ad libitum to food and water. The mice were divided into two dietary groups: chow diet (chow diet group, 70% calories from starch) and high-fat diet (HFC diet group, 60% fat and 1% cholesterol, Research Diet, #12492). All procedures were conducted in accordance with the Animal Welfare Legislation of China (Institutional Animal Care and Use Committee, Sun Yat-Sen University. Application No. 2023001490. Approval No. SYSU-IACUC-2023-001533). Mice on HFC diet were randomly assigned to four groups of equal mean body weight: HFC diet group (solvent administration), b2b group (10 or 20 mg/kg b2b administration) and orlistat (Yuanye Biotechnology Co., Ltd., Cat#S69030) group (20 mg/kg orlistat administration). All treatments were administered *via* gavage once daily. Compounds were prepared at a concentration of 2 mg/mL in 20% PEG-400 normal saline (*v*/*v*). Body weight and food intake were monitored daily. After 14 days treatment, mice were sacrificed, serum was collected, and tissues of interest were weighted, froze in liquid nitrogen, and fixed in 4% formaldehyde solution. Plasma chemical analysis was determined by technology company (BIOSSCI, China). The effects of anti-obesity of compound b2b on diet-induced-obese (DIO) mice were conducted followed by the produces[28]: Experiments of anti-obesity effects of compound b2b on diet-induced-obese (DIO) mice were completed in collaboration with Guangzhou Huateng Biomedical Technology Co., Ltd. and conducted followed by the produces: Male C57BL/6J mice (4−6 weeks old, Guangdong Medical Laboratory Animal Center) were housed under control conditions (22 ± 1 °C, 12 h light/dark cycle) with ad libitum to food and water. Mice were divided into two dietary groups: chow diet (CH, 70% calories from starch) and high-fat diet (60% fat and 1% cholesterol, Research Diet, #12492). The DIO mouse was established after 4 mouths of HFC feeding, defined by a body weight gain of over 20% compared to chow-fed mice)[60]. Then the DIO mice were randomly assigned to three groups of equal mean body weight: the HFC control group (solvent administration), and 20 mg/kg b2b group (b2b administration). Each group had six mice. Treatments were administered *via* intraperitoneal injection once daily. Compound b2b was prepared at concentrations of 2 mg/mL in 30% PEG-400 and 20% hydroxypropyl-β-cyclodextrin normal saline (*v*/*v*). Body weight and food intake were monitored daily. After 3 weeks of treatment with b2b, a glucose tolerance test (GTT) was performed as reported[61]. The mice were fasted for a period of 6 h and then treated with 2 g/kg glucose (Sigma, China) by gavage. The glucose level was determined at 0, 15, 30, 60, 90 and 120 min with a blood glucose monitor (Roche, USA). Blood samples for GTT were taken from the tail vein under local anesthesia with saline containing 2% lidocaine to ensure animal well-being and that it was not subjected to significant discomfort. After 5 weeks of treatment, mice were sacrificed, serum was collected, and tissues of interest were weighed, frozen in liquid nitrogen, and fixed in 4% formaldehyde solution. Plasma chemical analysis and immunohistochemical analysis were performed by a technology company (Biossci, China). Hematoxylin-eosin (H&E) staining of tissues was conducted by technology companies (Servicebio, China; Biossci, China).

5.9. Surface plasmon resonance (SPR) analysis

SPR was performed on a Biacore 8K system (GE Healthcare). Purified NAMPT were attached to the chip (CM5). Solutions of compounds were prepared with running buffer (1 × PBS, pH 7.4) through serial dilutions of stock solution, respectively. Several concentrations were injected simultaneously at a flow rate of 30 μL/min for 200 s of association phase, followed by 300 s of dissociation phase at 25 °C, using the multicycle kinetics injection mode. Data was analyzed with Biacore 8K evaluation software, using the affinity fit model for fitting data.

5.10. NAMPT expression

PT7-NAMPT (human)-6 × His (Commercial product), multisite-mutated PT7-NAMPT (human; Y188, Y240 and Q305 were mutated to Ala)-6 × His (Tsingke Biotech, Beijing) and multisite-mutated PT7-NAMPT (human; V242, P273 and I309 were mutated to Ala)-6 × His (Tsingke Biotech, Beijing) were grown in *Escherichia coli* BL21. The bacteria were grown at 37 °C for 8 h following induction with 0.5 mmol/L IPTG and continue cultured for at 20 °C for 16 h. The protein was purified through a nickel column. The purity of protein was checked *via* SDS-PAGE and Coomassie stain.

5.11. NAMPT enzyme activity assay

The orthogonal NAMPT assay was used to evaluate the enzymatic activity of compounds. For the Orthogonal NAMPT Assay: NMN Trapping. The method of Zhang et al.[52] was modified and miniaturized to establish an orthogonal assay for NAMPT activity. The assay uses the trapping of NMN by acetophenone in basic solution followed by acidification to form a fluorescent adduct (382 nm excitation, 445 nm emission). Reactions were performed at r.t. for 60 min in a 20 μL solution of 50 mmol/L Tris (pH 7.5), 5 mmol/L $MgCl_2$, 1 μmol/L NAMPT, 2 mmol/L ATP, 1 mmol/L NAM, 50 μmol/L PRPP, and test compound in 1% DMSO/buffer. After 60 min, to the reaction were added 20 μL of 20% acetophenone in DMSO and 20 μL of 2 mol/L KOH and then incubated on ice for 10 min. The reaction is quenched with 60 μL of 88% formic acid, incubated for 45 min at 37 °C, and read immediately. Fluorescence was measured with a microplate reader (Biotek, USA) at the condition (excitation wavelength, 382 nm; emission wavelength, 445 nm).

5.12. Cellular thermal shift assay (CETSA) assay

The confluence 3T3-L1 preadipocytes were incubated in a differentiation induction medium for 3 days. Subsequently, the cells were treated with the indicated concentrations of the compounds for 6 h in a 10% FBS/DMEM medium. The cells were harvested and washed with PBS, and the suspension was incubated at each temperature point from 35 to 75 °C for 3 min. The samples were freeze-thaw 3 times and centrifuged at 12,000 rpm at 4 °C for 20 min. The 80 μL supernatant was mixed with 20 μL of 5 × loading buffer and then separated on a 10% SDS-PAGE for immunoblotting assay.

5.13. Molecular docking

Docking studies were performed using the Schrodinger Maestro software. The crystal structure of NAMPT were obtained from the Protein Data Bank (PDB). The structure of compounds was generated using LigPrep module. Possible binding pockets were predicted by the ligand in the crystal structure. Docking analysis was first performed using the Glide module. 200 poses were

generated for each pocket, and post-docking minimization was performed. The models were visualized using the Pymol software package.

5.14. Transfection assay

The cells were transfected with mouse siRNA (100 nmol/L) using Lipofectamine3000 (Invitrogen, USA) according to the manufacturer's protocol. For 3T3-L1 cells, siRNA or negative control (NC) was added for two days between the stage of induction and differentiation. The sequence for siRNA or NC was shown in Supporting Information Table S5.

5.15. Statistical analysis

One-way ANOVA followed by two-tailed unpaired Student's *t*-tests were applied for multiple comparisons. The data were expressed as the mean ± SD. If $P < 0.05$, the difference was considered significant.

Acknowledgments

This study was supported by the National Natural Science Foundation of China (22507159, 81930098, 22377156, 22377153), Guangdong-macao Joint Science and Technology Innovation Project (2024A0505090023, China), Guangdong Basic and Applied Basic Research Foundation (2024A1515011751, China).

Author contributions

Zhi Jiang designed and performed compound synthesis and evaluation, target identification, and mechanistic investigations; Yixian Li conducted chemical synthesis and contributed to target discovery; Dandan Zhao implemented pharmacological evaluation and mechanistic studies; Lingzhen Xiao contributed to target discovery; Yu-tao Hu, Yuwei Lin, Shumin Xu and Jiachun Luo participated in compound efficacy assessments. Qingjiang Li, Shiliang Huang, Huihao Zhou and Jiaheng Tan provided assistance and guidance in experimental design and execution. Shuo-Bin Chen and Zhi-Shu Huang provided significant assistance, guidance, and financial support for experimental design and execution.

Conflicts of interest

The authors declare no conflicts of interests.

Appendix A. Supporting information

Supporting information to this article can be found online at https://doi.org/10.1016/j.apsb.2026.03.039.

References

1. Kusminski CM, Bickel PE, Scherer PE. Targeting adipose tissue in the treatment of obesity-associated diabetes. *Nat Rev Drug Discov* 2016; **15**:639−60.
2. Perdomo CM, Cohen RV, Sumithran P, Clément K, Frühbeck G. Contemporary medical, device, and surgical therapies for obesity in adults. *Lancet* 2023;**401**:1116−30.
3. Rubino F, Cummings DE, Eckel RH, Cohen RV, Wilding JPH, Brown WA, et al. Definition and diagnostic criteria of clinical obesity. *Lancet Diabetes Endocrinol* 2025;**13**:221−62.
4. Frayn KN, Arner P, Yki-Järvinen H. Fatty acid metabolism in adipose tissue, muscle and liver in health and disease. *Essays Biochem* 2006; **42**:89−103.
5. Ameer F, Scandiuzzi L, Hasnain S, Kalbacher H, Zaidi N. *De novo* lipogenesis in health and disease. *Metabolism* 2014;**63**:895−902.
6. Ghaben AL, Scherer PE. Adipogenesis and metabolic health. *Nat Rev Mol Cell Biol* 2019;**20**:242−58.
7. Batchuluun B, Pinkosky SL, Steinberg GR. Lipogenesis inhibitors: therapeutic opportunities and challenges. *Nat Rev Drug Discov* 2022; **21**:283−305.
8. He Q, Chen Y, Wang Z, He H, Yu P. Cellular uptake, metabolism and sensing of long-chain fatty acids. *Front Biosci (Landmark Ed)* 2023; **28**:10.
9. Jiang Y, Wang W, Wang H, Zhang X, Kong Y, Chen YQ, et al. ACSL1 positively regulates adipogenic differentiation. *Biochem Biophys Res Commun* 2024;**735**:150865.
10. Joseph R, Poschmann J, Sukarieh R, Too PG, Julien SG, Xu F, et al. ACSL1 is associated with fetal programming of insulin sensitivity and cellular lipid content. *Mol Endocrinol* 2015;**29**:909−20.
11. Mashek DG, Li LO, Coleman RA. Rat long-chain acyl-CoA synthetase mRNA, protein, and activity vary in tissue distribution and in response to diet. *J Lipid Res* 2006;**47**:2004−10.
12. Fagerberg L, Hallström BM, Oksvold P, Kampf C, Djureinovic D, Odeberg J, et al. Analysis of the human tissue-specific expression by genome-wide integration of transcriptomics and antibody-based proteomics. *Mol Cell Proteomics* 2014;**13**:397−406.
13. Hayashi K, Kondo N, Omori N, Yoshimoto R, Hato M, Shigaki S, et al. Discovery of a benzimidazole series as the first highly potent and selective ACSL1 inhibitors. *Bioorg Med Chem Lett* 2021;**33**:127722.
14. Dechandt CRP, Zuccolotto-dos-Reis FH, Teodoro BG, Fernandes AMAP, Eberlin MN, Kettelhut IC, et al. Triacsin C reduces lipid droplet formation and induces mitochondrial biogenesis in primary rat hepatocytes. *J Bioenerg Biomembr* 2017;**49**:399−411.
15. Covarrubias AJ, Perrone R, Grozio A, Verdin E. NAD+ metabolism and its roles in cellular processes during ageing. *Nat Rev Mol Cell Biol* 2021;**22**:119−41.
16. Xiao W, Wang RS, Handy DE, Loscalzo J. NAD(H) and NADP(H) redox couples and cellular energy metabolism. *Antioxidants Redox Signal* 2018;**28**:251−72.
17. Nikiforov A, Dölle C, Niere M, Ziegler M. Pathways and subcellular compartmentation of NAD biosynthesis in human cells: from ENTRY of extracellular precursors to mitochondrial NAD generation. *J Biol Chem* 2011;**286**:21767−78.
18. Yoshino J, Mills KF, Yoon MJ, Imai S. Nicotinamide mononucleotide, a key NAD+ intermediate, treats the pathophysiology of diet- and age-induced diabetes in mice. *Cell Metab* 2011;**14**:528−36.
19. Kwon SY, Park YJ. Function of NAD metabolism in white adipose tissue: lessons from mouse models. *Adipocyte* 2024;**13**:2313297.
20. Yoon MJ, Yoshida M, Johnson S, Takikawa A, Usui I, Tobe K, et al. SIRT1-mediated eNAMPT secretion from adipose tissue regulates hypothalamic NAD+ and function in mice. *Cell Metab* 2015;**21**: 706−17.
21. Yao H, Liu M, Wang L, Zu Y, Wu C, Li C, et al. Discovery of small-molecule activators of nicotinamide phosphoribosyltransferase (NAMPT) and their preclinical neuroprotective activity. *Cell Res* 2022;**32**:570−84.
22. Gardell SJ, Hopf M, Khan A, Dispagna M, Hampton SE, Falter R, et al. Boosting NAD(+) with a small molecule that activates NAMPT. *Nat Commun* 2019;**10**:3241.
23. Wang L, Liu M, Zu Y, Yao H, Wu C, Zhang R, et al. Optimization of NAMPT activators to achieve *in vivo* neuroprotective efficacy. *Eur J Med Chem* 2022;**236**:114260.
24. Cheng J, Zhang J, He S, Li M, Dong G, Sheng C. Photoswitchable PROTACs for reversible and spatiotemporal regulation of NAMPT and NAD(+). *Angew Chem Int Ed Engl* 2024;**63**:e202315997.

25. Rao Y, Yu H, Gao L, Lu YT, Xu Z, Liu H, et al. Natural alkaloid bouchardatine ameliorates metabolic disorders in high-fat diet-fed mice by stimulating the sirtuin 1/liver kinase B-1/AMPK axis. *Br J Pharmacol* 2017;**174**:2457−70.
26. Jiang Z, Hu YT, Guo SY, Li YX, Zhao DD, Wei LY, et al. Development of novel N-acylhydrazone derivatives with high anti-obesity activity and improved safety by exploring the pharmaceutical properties of aldehyde group. *J Med Chem* 2024;**67**:12439−58.
27. O'Brien PJ, Siraki AG, Shangari N. Aldehyde sources, metabolism, molecular toxicity mechanisms, and possible effects on human health. *Crit Rev Toxicol* 2005;**35**:609−62.
28. Uehling MR, King RP, Krska SW, Cernak T, Buchwald SL. Pharmaceutical diversification *via* palladium oxidative addition complexes. *Science* 2019;**363**:405−8.
29. Jiang Z, Zhao DD, Hu YT, Rao Y, Guo SY, Xu YH, et al. Palladium oxidative addition complex-enabled synthesis of amino-substituted indolyl-4(3*H*)-quinazolinones and their antitumor activity evaluation. *Org Biomol Chem* 2022;**20**:553−7.
30. Guru A, Issac PK, Velayutham M, Saraswathi NT, Arshad A, Arockiaraj J. Molecular mechanism of down-regulating adipogenic transcription factors in 3T3-L1 adipocyte cells by bioactive anti-adipogenic compounds. *Mol Biol Rep* 2021;**48**:743−61.
31. Sun K, Kusminski CM, Scherer PE. Adipose tissue remodeling and obesity. *J Clin Investig* 2011;**121**:2094−101.
32. Seebacher F, Zeigerer A, Kory N, Krahmer N. Hepatic lipid droplet homeostasis and fatty liver disease. *Semin Cell Dev Biol* 2020;**108**: 72−81.
33. Huang Q, Ru Y, Luo Y, Luo X, Liu D, Ma Y, et al. Identification of a targeted ACSL4 inhibitor to treat ferroptosis-related diseases. *Sci Adv* 2024;**10**. eadk1200.
34. Smith E, Collins I. Photoaffinity labeling in target- and binding-site identification. *Future Med Chem* 2015;**7**:159−83.
35. Okabe K, Nawaz A, Nishida Y, Yaku K, Usui I, Tobe K, et al. NAD+ metabolism regulates preadipocyte differentiation by enhancing α-ketoglutarate-mediated histone H3K9 demethylation at the PPARγ promoter. *Front Cell Dev Biol* 2020;**8**:586179.
36. Cantó C, Houtkooper RH, Pirinen E, Youn DY, Oosterveer MH, Cen Y, et al. The NAD(+) precursor nicotinamide riboside enhances oxidative metabolism and protects against high-fat diet-induced obesity. *Cell Metab* 2012;**15**:838−47.
37. Kane AE, Sinclair DA. Sirtuins and NAD(+) in the development and treatment of metabolic and cardiovascular diseases. *Circ Res* 2018; **123**:868−85.
38. GBD 2021 Adult BMI Collaborators. Global, regional, and national prevalence of adult overweight and obesity, 1990−2021, with forecasts to 2050: a forecasting study for the global Burden of Disease Study 2021. *Lancet* 2025;**405**:813−38.
39. Kolotkin RL, Andersen JR. A systematic review of reviews: exploring the relationship between obesity, weight loss and health-related quality of life. *Clin Obes* 2017;**7**:273−89.
40. Lupianez-Merly C, Dilmaghani S, Vosoughi K, Camilleri M. Review article: pharmacologic management of obesity−updates on approved medications, indications and risks. *Aliment Pharmacol Ther* 2024;**59**: 475−91.
41. Williams HD, Trevaskis NL, Charman SA, Shanker RM, Charman WN, Pouton CW, et al. Strategies to address low drug solubility in discovery and development. *Pharmacol Rev* 2013;**65**: 315−499.
42. Porter CJ, Trevaskis NL, Charman WN. Lipids and lipid-based formulations: optimizing the oral delivery of lipophilic drugs. *Nat Rev Drug Discov* 2007;**6**:231−48.
43. Stromsdorfer KL, Yamaguchi S, Yoon MJ, Moseley AC, Franczyk MP, Kelly SC, et al. NAMPT-mediated NAD+ biosynthesis in adipocytes regulates adipose tissue function and multi-organ insulin sensitivity in mice. *Cell Rep* 2016;**16**:1851−60.
44. Uddin GM, Youngson NA, Sinclair DA, Morris MJ. Head to head comparison of short-term treatment with the NAD+ precursor nicotinamide mononucleotide (NMN) and 6 weeks of exercise in obese female mice. *Front Pharmacol* 2016;**19**:258.
45. Kim MB, Pham TX, vanLuling M, Kostour V, Kang H, Corvino O, et al. Nicotinamide riboside supplementation exerts an anti-obesity effect and prevents inflammation and fibrosis in white adipose tissue of female diet-induced obesity mice. *J Nutr Biochem* 2022;**107**: 109058.
46. Akiu M, Tsuji T, Iida K, Sogawa Y, Terayama K, Yokoyama M, et al. Discovery of DS68702229 as a potent, orally available NAMPT (nicotinamide phosphoribosyltransferase) activator. *Chem Pharm Bull (Tokyo)* 2021;**69**:1110−22.
47. Diraison F, Dusserre E, Vidal H, Sothier M, Beylot M. Increased hepatic lipogenesis but decreased expression of lipogenic gene in adipose tissue in human obesity. *Am J Physiol Endocrinol Metab* 2002;**282**:E46−51.
48. Ellis JM, Li LO, Wu PC, Koves TR, Ilkayeva O, Stevens RD, et al. Adipose acyl-CoA synthetase-1 directs fatty acids toward beta-oxidation and is required for cold thermogenesis. *Cell Metab* 2010; **12**:53−64.
49. Ramakrishnan S, Mooli RGR, Han Y, Fiorenza E, Fiorenza E, Kumar S, et al. Hepatic ketogenesis regulates lipid homeostasis *via* ACSL1-mediated fatty acid partitioning. *Res Sq [Preprint]* 2023;**18**. rs.3.rs-3147009.
50. Li LO, Mashek DG, An J, Doughman SD, Newgard CB, Coleman RA. Overexpression of rat long chain acyl-coa synthetase 1 alters fatty acid metabolism in rat primary hepatocytes. *J Biol Chem* 2006;**281**: 37246−55.
51. Li LO, Klett EL, Coleman RA. Acyl-CoA synthesis, lipid metabolism and lipotoxicity. *Biochim Biophys Acta* 2010;**1801**:246−51.
52. Shen Z, Ratia K, Krider I, Ackerman-Berrier M, Penton C, Musku SR, et al. Optimization, and structure-activity relationships of nicotinamide phosphoribosyltransferase (NAMPT) positive allosteric modulators (N-PAMs). *J Med Chem* 2023;**66**:16704−27.
53. Banks AS, Kon N, Knight C, Matsumoto M, Gutiérrez-Juárez R, Rossetti L, et al. SirT1 gain of function increases energy efficiency and prevents diabetes in mice. *Cell Metab* 2008;**8**:333−41.
54. Yamaguchi S, Franczyk MP, Chondronikola M, Qi N, Gunawardana SC, Stromsdorfer KL, et al. Adipose tissue NAD+ biosynthesis is required for regulating adaptive thermogenesis and whole-body energy homeostasis in mice. *Proc Natl Acad Sci U S A* 2019;**116**:23822−8.
55. Li BY, Peng WQ, Liu Y, Guo L, Tang QQ. HIGD1A links SIRT1 activity to adipose browning by inhibiting the ROS/DNA damage pathway. *Cell Rep* 2023;**42**:112731.
56. Yang X, Zhang X, Yang Z, Zhang Q, Hao W, Pang Y, et al. Transcriptional regulation associated with subcutaneous adipogenesis in porcine ACSL1 gene. *Biomolecules* 2023;**13**:1057.
57. Fu H, Han X, Guo W, Zhao X, Zhao X, Yu C, et al. Cystathionine-γ-lyase contributes to tamoxifen resistance, and the compound I194496 alleviates this effect by inhibiting the PPARγ/ACSL1/STAT3 signalling pathway in oestrogen receptor-positive breast cancer. *Sci Rep* 2024;**14**:22988.
58. Zeng XY, Zhou X, Xu J, Chan SMH, Xue CL, Molero JC, et al. Screening for the efficacy on lipid accumulation in 3T3-L1 cells is an effective tool for the identification of new anti-diabetic compounds. *Biochem Pharmacol* 2012;**84**:830−7.
59. Wei LY, Lin YW, Luo JC, Li YX, Hu YT, Guo SY, et al. Design, synthesis and structure−activity relationship of novel 2-pyrimidinylindole derivatives as orally available anti-obesity agents. *Eur J Med Chem* 2024;**277**:116773.
60. Gwon MH, Im YS, Seo AR, Kim KY, Moon HR, Yun JM. Phenethyl isothiocyanate protects against high fat/cholesterol diet-Induced obesity and atherosclerosis in C57BL/6 mice. *Nutrients* 2020;**12**:3657.
61. Pollard AE, Martins L, Muckett PJ, Khadayate S, Bornot A, Clausen M, et al. AMPK activation protects against diet induced obesity through Ucp1-independent thermogenesis in subcutaneous white adipose tissue. *Nat Metab* 2019;**1**:340−9.